# Spatiotopic Organization in Human Superior Colliculus Observed with fMRI

Richard M. DuBois* and Mark S. Cohen†

*Neuroscience IDP and †Department of Neurology, University of California, Los Angeles, 660 Charles E. Young Drive South, Los Angeles, California 90095

**Spatiotopy is a fundamental organizing principle of the visual brain. Using functional magnetic resonance imaging, we have demonstrated reliable data, consistent with spatiotopic organization in the human superior colliculi. Five subjects underwent cardiac-triggered echo-planar image acquisition, during which they viewed alternating left and right visual hemifield stimulation. Intensity variations from the variable TR were removed, and the data were evaluated for correlation with the lateralized stimulus. The data indicate a strongly preferential response of the left superior colliculus to the right side of visual space, and vice versa. This is consistent with previous findings in animal systems and confirms the existence of spatiotopy in the human superior colliculus.** © 2000 Academic Press

*Key Words:* colliculus; retinotopy; spatiotopy; fMRI; cardiac, gating.

The ability of humans and other animals to perceive the spatial relationships of their body to its surroundings is essential for successful navigation in their environment. This perception is mediated by a variety of cortical and subcortical centers in the brain, including visual cortex, parietal cortex, and the superior colliculus (SC) (Andersen *et al.,* 1985; Battaglini *et al.,* 1996; Colby *et al.,* 1995; Harris *et al.,* 1980; Maunsell, 1995). To understand better how the brain uses these centers to form a perceptual map of external space, it is critical to first define their functional organization. Without this, we cannot hope to comprehend the mechanism of spatial perception.

The organization of the visual cortex has been studied for decades by careful observation of lesions (De Weerd *et al.,* 1993; Flandrin *et al.,* 1992; Henschen 1893; Holmes, 1918, 1931, 1945; Hughes and Sprague, 1986), electrophysiology (Hubel and Wiesel, 1962), and, more recently, noninvasive functional imaging methods such as positron emission tomography (PET) (Fox *et al.,* 1987) and functional magnetic resonance imaging (fMRI) (Engel *et al.,* 1997; Sereno *et al.,* 1995). Investigators have found clear evidence of retinotopy in many subregions within the visual cortex, including most of the early visual areas (DeYoe *et al.,* 1996; Engel *et al.,* 1997; Sereno *et al.,* 1994, 1995; Van Essen *et al.,* 1990). The parietal cortex, especially the posterior and lateral inferior areas, has also been shown to be involved in spatial awareness, although its organization and contribution are somewhat less well understood (Andersen, 1995; Colby *et al.,* 1995, 1996). Topographic representation appears to be the rule for most other sensory modalities (with the exception of olfaction— see Freeman and Baird (1987)).

The organization of the human SC, however, is not yet well known. Its connections to the visual stream from the retina, visual cortex, and parietal cortex (Colby *et al.,* 1995; Sparks, 1988) support the interpretation that it serves as an important integrative visual center. Retinotopic organization in the SC in many lower vertebrates has been demonstrated amply (Harris *et al.,* 1980; Sparks, 1988; Sprague *et al.,* 1970) and has been studied in ferrets (Quevedo *et al.,* 1996), frogs (Bandarchi *et al.,* 1994; Somogyvari *et al.,* 1998), fish (Pinganaud *et al.,* 1983; Trowe *et al.,* 1996), wallabies (James *et al.,* 1993; Marotte, 1990), and many other species and seems to be directly analogous to that found in the avian optic tectum. In primates, there is also considerable evidence supporting retinotopy in SC (Cynader and Berman, 1972; Lane *et al.,* 1973), although there is little or no evidence specifically in humans. Many studies have also suggested an important role of the SC in visual saccades and tracking and in supplying a "motor map" (Lee *et al.,* 1988; Massone, 1994; Mays and Sparks, 1980; Moschovakis, 1996; Sparks and Jay, 1986; Sparks *et al.,* 1990; Sparks and Mays, 1980, 1983), which would be relevant to the construction of an internal "map" of external space. Unfortunately, it has been difficult to observe this structure in humans, *in vivo.* Its location at the rear of the midbrain renders it inaccessible to electrophysiological probes, even during brain surgery, and its small size and movement with blood pulsation in the brainstem have made observation with noninvasive imaging methods difficult (Poncelet *et al.,* 1992). A method dem-

onstrated by Guimaraes *et al.* (1998) used cardiac triggering of image acquisition and a novel intensity correction technique to make imaging of the human inferior colliculus possible. A very similar technique is used in this study.

The use of high-field-strength MRI devices has made functional imaging of small regions possible (Cohen *et al.,* 1996). As signal strength in fMRI scales roughly linearly with field strength, with such instruments we can increase spatial resolution while maintaining a signal-to-noise ratio adequate to produce useful images. The present study utilized fMRI at 3 T to acquire images that give each SC a spatial extent of several pixels (see Results, Fig. 1), making it possible to observe evidence of blood flow response within them without substantial increases in scan time due to averaging of repeated scans.

## METHODS

### Scan Protocol

Six subjects (three male, three female, mean age 27.2 years) were studied using fMRI. None reported a history of trauma or abnormality, and all provided informed consent according to the guidelines of the UCLA Human Subjects Protection Committee. One male subject was found to have a subarachnoid cerebellar cyst and was excluded from further analysis. MR imaging was performed on a 3T General Electric Signa scanner (GE Medical Systems, Waukesha, WI) with gradient and image processing hardware developed by Advanced NMR Systems, Inc. Prior to functional scanning, the instrument was shimmed using an echo-planar imaging (EPI)-based procedure (Reese *et al.,* 1995), followed by acquisition of baseline structural images (FSE, TE 40, TR 4000, 20 cm FOV, 256 × 256, 4 mm thick/skip 1). We then acquired high-resolution EPI structural "localizer" images of the three to five slices under study (TE 55, TR 4000, 20 cm FOV, 128 × 128, 4 NEX). These oblique coronal slices were chosen to include a plane passing through the superior and inferior colliculi, 3.0 mm thick with 0.0-mm spacing, covering the entire volume of the superior colliculi; these images have an in-plane resolution of 1.56 mm. We then collected a set of images at the same locations at TRs of 1.0 and 10.0 s using EPI gradient echo scan sequences (128 × 128, 20 cm FOV, 1 NEX). Finally, we collected a set of 90 functional images using gradient echo EPI (TE 30 ms, 128 × 128, 20 cm FOV, 1 NEX), with repetition time (TR) determined by subject heart rate as monitored by a pulse oximeter. The average heart rate was 68.4 beats per minute and generally varied between 60 and 80 beats per minute, giving TRs of 2.25 to 3 s (average 2.63). During this acquisition, visual stimuli were presented to the subjects through magnet-compatible LCD video goggles (Resonance

Technology, Northridge, CA). Our stimuli consisted of 30 s of rest, during which subjects maintained gaze fixation on a central cross on a gray screen. This was followed by 30-s blocks of visual stimulation using a half-circle of checkerboard with features inverting at 8 Hz, with blocks alternating between left and right hemifields. During hemifield stimulation blocks, the subject was instructed to maintain gaze fixation on a central cross. The number of TRs during each stimulus phase (left or right) varied due to the cardiac gating and so was recorded by hand. In addition, the exact timing of scan acquisition was recorded on a Macintosh computer by detection of a scanner trigger pulse sent with the acquisition of each slice. This pulse was detected and digitized at 22.05 kHz (SoundEdit 16, Macromedia, San Francisco, CA) for later use in T1 correction.

### T1 Correction

We determined the TR of each time point automatically based on the scan timing record and calculated the mean TR of the scan for each subject. The T1 of each voxel in the imaged volume was determined by comparing the intensity of each voxel in the imaged volume at the two different TRs (1.0 and 10.0 s). Signal intensity at a given T1 and TR is determined as:

$$SI = k(1 - e^{-TR/T1}). \tag{1}$$

Given two TRs (and thus two intensities) for a single voxel, one can calculate its T1 by combining the two signal intensity equations, as follows:

$$\frac{SI_1}{SI_2} = \frac{1 - e^{-TR_1/T1}}{1 - e^{-TR_2/T1}}. \tag{2}$$

This can be solved readily for T1 if the second TR is considered infinite (a valid assumption in our case, as a TR of 10.0 s produces 99.98% signal recovery in a voxel with T1 of 1.2)

$$T1 = \frac{-TR_1}{\ln(1 - SI_1/SI_2)}, \tag{3}$$

which allows determination of T1 from the two intensities.

Once we had created this T1 map, we used it to determine intensity variations at each voxel arising from variable TR. We calculated the average TR for an entire imaging session, as well as the difference between the actual intensity and the hypothetical intensity (at average TR) for each voxel at each time point. We then corrected the intensity of each voxel to remove that difference, so that all variations based on variable

TR were eliminated. This approach preserves the T2* components of the blood oxygenation level-dependent (BOLD) signal.

To assess the validity and efficacy of this method, we performed two separate tests. In the first, we performed EPI scanning on a phantom at three different TRs using the same pulse sequence and slice parameters as in the human functional scanning and then concatenated these scans into a single file, simulating a single imaging session. Five images were taken at TRs of 1.0, 2.0, and 5.0 s, for a total of 15 images. These were then subjected to the T1-based intensity correction procedure, correcting all intensities to the mean TR of 2.79 s (the first image is ignored, as its TR is not easily determined).

The second test was performed on a human volunteer. The subject performed a standard hand motor task during cardiac-triggered EPI scanning of the upper areas of the brain. This time series was then subjected to a standard correlation analysis substantially identical to that used in this report, before and after T1 correction.

### Validation

To test the efficacy of the procedure, an ROI that covered a large portion of the center of the phantom was selected. By choosing a large area, we minimized the effect of thermal noise in any given pixel, which might contribute to image intensity variations over time and within each image. We then calculated the mean intensity within the ROI for each time point and calculated the standard deviation of intensity over images 2–15 (the first image was not modified by the T1 correction procedure, as its TR is not always known).

### Image Analysis

The corrected data series was then used to create functional maps by evaluating the correlation of the signal intensity changes with a model of predicted response. The latter was derived by convolution of an empirical impulse response (Savoy *et al.,* 1994) with stimulus timing (Cohen, 1997). Regions of interest (ROIs) covering the left and right superior colliculi were determined by visual inspection of the high-resolution structural EPI images, without reference to the functional data (Results, Fig. 1). We determined these ROIs by manually creating a rectangle on either the right or the left SC in each slice in which it was visible. These rectangles contained all visible SC tissue, while excluding as much of the surrounding fluid and non-SC tissue as possible.

We subjected the functional data to a Hanning smoothing procedure, using a $3 \times 3$ pixel kernel. We then determined the correlation between the actual pixel intensity time course and the stimulus timing using software developed in-house. For subsequent
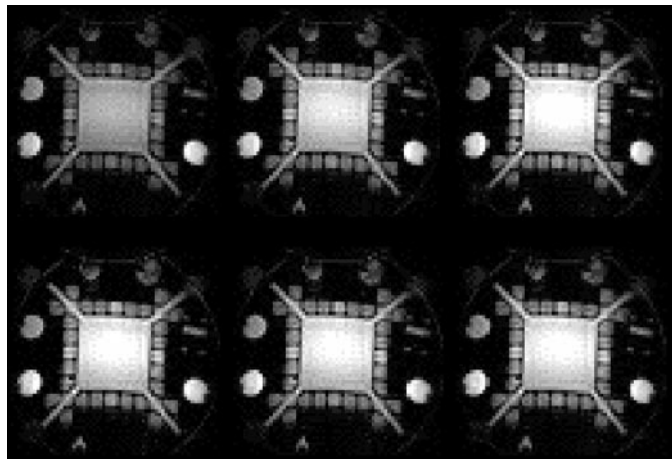


**FIG. 1.** Demonstration of T1 correction. The top three images are of a phantom, taken at TRs of 1.0, 2.0, and 5.0 s, from left to right. The bottom three images are the same images after T1 correction to the mean TR of 2.79 s.

analysis, we considered only pixels in these ROIs whose signal intensity time course was correlated with either left or right impulse response models to greater than 0.25 (Pearson's linear correlation coefficient). The number of pixels exceeding threshold in each of four conditions (left colliculus correlated to right hemifield stimulation, left colliculus/left hemifield, right colliculus/right hemifield, and right colliculus/left hemifield) was recorded, and we obtained an average intensity record at all time points for those pixels.

Because the exact timing of the intensity record differed for each stimulus cycle, we interpolated the intensity time course record to 0.1-s resolution. The interpolated intensities at each integer second were then extracted and used for all further analysis. Each 60-s cycle of right and left stimulation was averaged within each subject, producing one 60-s time course for each subject representing average intensity over the right–left stimulus cycle.

To quantify the laterality of responses, we calculated a laterality index as

$$\frac{\text{Voxels in left SC} - \text{Voxels in right SC}}{\text{Voxels in left SC} + \text{Voxels in right SC}}, \quad (4)$$

where "voxels" refers to suprathreshold responding voxels, for both right and left hemifield stimulation. Thus, a value of 1.0 would indicate entirely left SC response, $-1.0$ would indicate entirely right SC, and NR would indicate no response of either left or right SC for that hemifield stimulation.

### Across Subject Analysis

We created a new time course for each subject, using the averaged intensities at integer seconds to enable
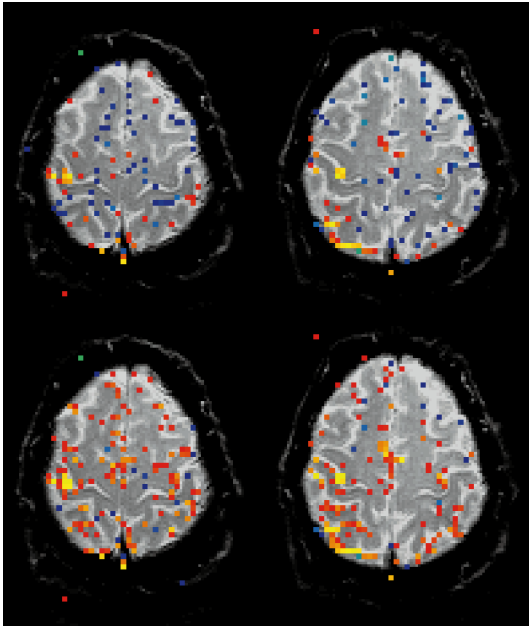
**FIG. 2.** Effects of T1 correction on cardiac-triggered fMRI. A subject performed a blocked finger opposition task during cardiac-triggered echo-planar imaging. All images were analyzed for correlation with performance of the task. Red to yellow indicates increasing positive correlation, while blue indicates negative correlation. The top two slices are uncorrected for intensity variation, while the bottom two images are of the same slices after correction.

cross-subject comparisons. The time courses for all five subjects were normalized to unit amplitude, such that the difference between average intensities in right and left stimulation phases was equal. The intensity value at each time point was then averaged across subjects to produce an across-subject average in each condition. This approach relies on *a priori* assignment of ROIs within the SC rather than spatial realignment (e.g., by AIR or SPM).

## RESULTS

The results of the intensity correction test involving the phantom are shown in Fig. 1. At the top are uncorrected images obtained at 1.0-, 2.0-, and 5.0-s TRs, while at the bottom are the same three images after correction. Analysis of the variation in intensity over time in the corrected images revealed a standard deviation of 1.53% of the mean intensity. This can be compared to a standard deviation of 0.49% of the mean intensity in a series of images in the same phantom taken at a static TR of 2.7 s. Both of these variability measures are small when compared to a 17% standard deviation in the uncorrected images, indicating that the image correction procedure is effective at reducing interimage variability due to time-dependent intensity variations.

Figure 2 shows the results of the T1 intensity cor-

rection in the hand-motor task. On the top are activation maps showing response during hand movement compared to rest from an uncorrected image. The images on the bottom are the results of precisely the same analysis on the corrected image. Note that observed correlations are higher (brighter reds and oranges), with several areas of activation that were hidden in the uncorrected images revealed by correction.

Figure 3 is an illustration of the ROIs covering left and right SC in a representative subject (PD). Note that the location of the SC is defined easily in this figure. This was true for all subjects, confirming that the voxel time courses obtained were from the SC. As mentioned previously, the apparent difference in ROI size is due to the tilt of the slice planes, as well as possibly inherent asymmetry in shape and size between the colliculi.

The number of suprathreshold voxels in all four conditions is shown in Table 1, along with the number of voxels in the ROIs and the laterality index for responses. These data indicate strong evidence of lateralization of response within the colliculi. There were significantly more suprathreshold voxels in contralateral than ipsilateral conditions ($P < 0.003$, one-tailed two-sample unequal variance Student's $t$ test). Analysis of the same data without T1 correction found no significant difference in the number of suprathreshold voxels in ipsilateral versus contralateral conditions ($P < 0.43$). The mean number of suprathreshold voxels and calculated laterality index for data without T1
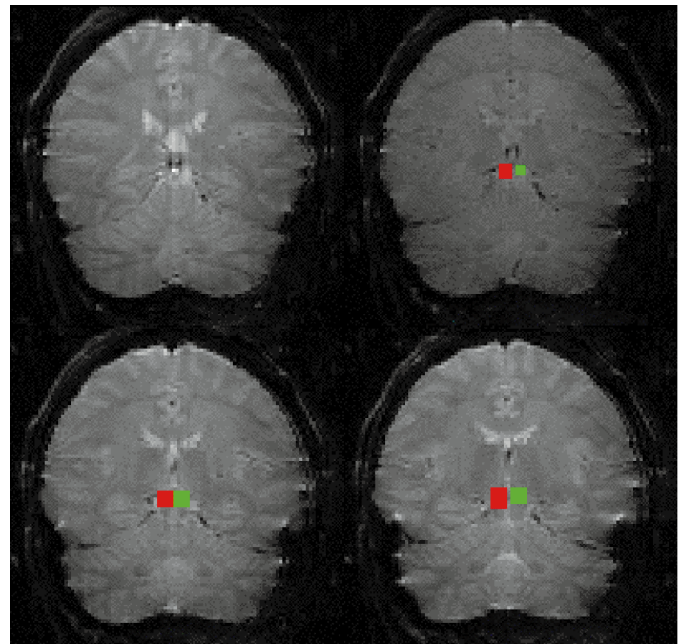


**FIG. 3.** Illustration of ROI selection. Data shown are from a representative subject (PD). ROIs covering the left superior colliculus (green) and right superior colliculus (red) are shown.

## TABLE 1
### Number of Suprathreshold Voxels and Laterality Index

| Subject | ROI size | Ipsilateral | | Contralateral | | Rest | | Laterality index | | |
|---|---|---|---|---|---|---|---|---|---|---|
| | | LC/LS | RC/RS | LC/RS | RC/LS | LC | RC | Left | Rest | Right |
| JC | 77/70 | 0 | 2 | 8 | 0 | 2 | 0 | NR | 1.0 | 0.6 |
| SD | 81/75 | 3 | 0 | 9 | 8 | 8 | 0 | −0.45 | 1.0 | 1.0 |
| PD | 59/71 | 0 | 1 | 4 | 12 | 1 | 9 | −1.0 | −0.8 | 0.6 |
| KH | 108/81 | 0 | 0 | 2 | 4 | 0 | 0 | −1.0 | NR | 1.0 |
| KN | 120/122 | 2 | 1 | 3 | 2 | 2 | 8 | 0.0 | −0.6 | 0.5 |
| Mean | 89/83.8 | 1.0 | 0.8 | 5.2 | 5.2 | 2.6 | 3.4 | −0.51 | 0.15 | 0.74 |
| Without T1 correction | | 3.0 | 0.2 | 1.6 | 2.2 | 18.4 | 15.8 | 0.54 | 0.08 | 0.2 |

*Note.* All conditions are shown. Number of voxels in ROI shown as left/right. Laterality index was calculated as described in Eq. (4). Rest condition represents results of analysis for "activation" during initial rest period only. Last row represents mean values after analysis without T1 correction (individual values not shown). LC, left superior colliculus; RC, right superior colliculus; LS, left hemifield stimulation; RS, right hemifield stimulation.

correction are shown in the last row of the table. Individual values for uncorrected analysis are not shown.

Figure 4 illustrates representative time courses (subject SD) in all conditions for which suprathreshold voxels were found. In the scans of this subject, there were four blocks of right hemifield stimulation and three complete blocks of left hemifield stimulation, with one partial left block at the end terminated by the completion of the scan. Note that the rightmost time course shown in Fig. 4, taken from the few ipsilateral pixels which exceeded threshold in this subject, is considerably noisier.

Across-subject averaged time courses for the two contralateral and two ipsilateral conditions are shown in Fig. 5. These indicate that the contralateral response shape was consistent in all subjects. In addition, the time course closely follows the hemodynamic response model, shown in the thinner line. This indicates that the observed response is most likely a true blood flow response, rather than signal variation arising from artifact, noise, or intensity correction procedures.
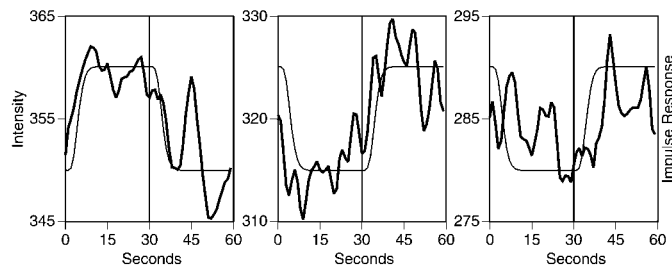
## DISCUSSION

Retinotopic and spatiotopic organization have been observed ubiquitously throughout the brains of vertebrate animals; it is seen even where spatial location is not inherently present in incoming stimuli and must be calculated. For example, the early auditory areas of several varieties of bat are known to reflect sound source localization (Suga and O'Neill, 1979). Even so, the functional significance of such organization is far from clear. On the one hand, the proximity on cortex of related information would seem to offer a computa-
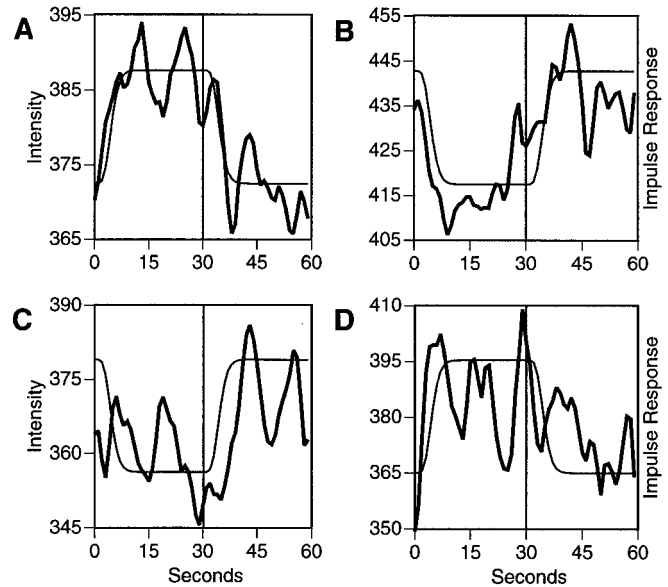
**FIG. 4.** Average time courses in a single subject. Intensity time courses for a representative subject (SD) in the three conditions for which suprathreshold voxels were found. From left to right: two contralateral conditions (left colliculus responding to right hemifield, right colliculus responding to left hemifield) and one ipsilateral condition (left colliculus responding to left hemifield). The thick lines are the intensity time courses. Estimated hemodynamic response is shown by the thin lines.

**FIG. 5.** Average time courses across subjects. Contralateral (A and B) and ipsilateral (C and D) conditions are shown. (A) Left superior colliculus responding to right hemifield stimulation. (B) Right superior colliculus responding to left hemifield stimulation. (C) Left colliculus, left hemifield. (D) Right colliculus, right hemifield. Thick lines are the intensity time courses. Estimated hemodynamic response is shown by the thin lines.

tional advantage. It is easy to see, for example, that local inhibition of neurons within a retinotopically organized cortex can lead to the formation of the "simple" cell activity observed by Hubel and Wiesel (1962). On the other hand, it is known that, in some cases, human albinos have patches of ipsilateral representations on the visual cortex, yet lack profound visual deficits (Guillery *et al.,* 1975; Hedera *et al.,* 1994), suggesting that nonlocal interactions might lead to the same functional effects. Further, the retinotopic organization of normal cortex is relatively crude, even in the striate cortex, where the receptive fields of magnocellular and parvocellular components overlap in patches and thus violate retinotopy over short distances (Livingstone and Hubel, 1987). In fact, it may be energetically favorable in neural development for cortical areas to have a simple point to point mapping to afferent sources (e.g., the retina).

Further, in many brain areas, spatiotopy is not a stable organization principle. In experiments with skin grafts, Merzenich *et al.* (1983) showed that the primate somatosensory cortex was capable of reorganization that distorted the point to point mapping of the periphery onto the cortex. On the motor cortex, the local spatiotopic organization is also arranged dynamically, apparently according to functional semantics. The studies of Pascual-Leone, for example, suggested that such maps may become altered over the course of minutes to hours (Pascual-Leone *et al.,* 1994a, b).

There are a few structures, however, where spatiotopy apparently underlies brain function. In their now classic work studying the optic tectum of the barn owl (*Tyto alba*), Knudsen and colleagues showed that this structure underwent plastic changes in organization when sensory input was altered (Knudsen, 1985; Knudsen and Brainard, 1991). Specifically, the spatiotopic maps of the visual and auditory world were kept in physical alignment in the tectum, even when the visual inputs were distorted. It is in large part these results that have motivated us to study the organization of the colliculus in humans, as we expect that retinotopy has substantial functional consequences.

If we assume that retinotopy and other spatiotopy have functional value, how can we investigate the role of such mapping? We believe that fMRI provides the needed window for this sort of observation.

Compensating for pulsatile motion required special methods. While cardiac triggering can eliminate pulsatile motion effects per se, it introduces variations in signal intensity in the time series. This is due to the dependence of the MR signal on time between excitations (TR), which, in single-shot EPI, is the time between images. Signal intensity is determined by the formula in Eq. (1), taking the derivative of which produces the result that

$$\frac{d\mathrm{SI}}{d(\mathrm{TR})} = \frac{e^{-\mathrm{TR/T1}}}{\mathrm{T1}}. \qquad (5)$$

This T1- and TR-dependent variation can mask the small intensity variations that characterize BOLD contrast signal in fMRI, eliminating the advantages of cardiac gated fMRI. In this experiment, we used a software-based T1 correction algorithm to compensate for the intensity variations produced by a variable TR. Analysis without these corrections risks masking of valid blood flow changes and introduction of false changes from these intensity variations. We believe that our approach is similar to that of Guimaraes *et al.* (1998). We observed postcorrection variation over time slightly greater than that seen in a series of images with a static TR, indicating quantitatively that the correction algorithm removes nearly all of the intensity variation. The remaining variation (standard deviation 1.5% of mean) is well below our roughly 3–4% functional signal change, confirming that our observed fMRI responses are not an artifact from the correction procedure.

These findings of contralateral response of the SC—which, while not themselves proof of retinotopy, strongly suggest a retinotopic organization—provide further evidence that the superior colliculus is an important center for visuospatial perception. In addition, we have shown that it is possible to use noninvasive imaging to analyze the organization of the SC in normal humans, making it possible to further investigate the contributions of this and other small nuclei to the phenomenon of perception.

## ACKNOWLEDGMENTS

## REFERENCES

Andersen, R. A. 1995. Encoding of intention and spatial location in the posterior parietal cortex. *Cereb. Cortex* **5:**457–469.

Andersen, R. A., Essick, G. K., and Siegel, R. M. 1985. Encoding of spatial location by posterior parietal neurons. *Science* **230:**456–458.

Bandarchi, J., Scherer, W. J., and Udin, S. B. 1994. Acceleration by NMDA treatment of visually induced map reorganization in juvenile *Xenopus* after larval eye rotation. *J. Neurobiol.* **25:**451–460.

Battaglini, P. P., Galletti, C., and Fattori, P. 1996. Cortical mechanisms for visual perception of object motion and position in space. *Behav. Brain Res.* **76:**143–154.

Cohen, M. S. 1997. Parametric analysis of fMRI data using linear systems methods. *NeuroImage* **6:**93–103.

Cohen, M. S., Kelley, D. A., Rohan, M. L., Roemer, P. A. (1996). An MR instrument optimized for intracranial neuroimaging. *Hum. Brain Mapping* **96:**P1A1–007. Boston, MA.

Colby, C., Duhamel, J.-R., and Goldberg, M. 1996. Multiple parietal representations of space. In *Brain Theory: Biological Basis and Computational Principles* (A. Aertsen and V. Braitenberg, Eds.), pp. 37–52. Elsevier, Amsterdam/New York.

Colby, C. L., Duhamel, J. R., and Goldberg, M. E. 1995. Oculocentric spatial representation in parietal cortex. *Cereb. Cortex* **5:**470–481.

Cynader, M., and Berman, N. 1972. Receptive-field organization of monkey superior colliculus. *J. Neurophysiol.* **35:**187–201.

De Weerd, P., Sprague, J. M., Raiguel, S., Vandenbussche, E., and Orban, G. A. 1993. Effects of visual cortex lesions on orientation discrimination of illusory contours in the cat. *Eur. J. Neurosci.* **5:**1695–1710.

DeYoe, E. A., Carman, G. J., Bandettini, P., Glickman, S., Wieser, J., Cox, R., Miller, D., and Neitz, J. 1996. Mapping striate and extrastriate visual areas in human cerebral cortex. *Proc. Natl. Acad. Sci. USA* **93:**2382–2386.

Engel, S. A., Glover, G. H., and Wandell, B. A. 1997. Retinotopic organization in human visual cortex and the spatial precision of functional MRI. *Cereb. Cortex* **7:**181–192.

Flandrin, J. M., Courjon, J. H., Orban, G. A., and Sprague, J. M. 1992. Long-term impairment of cat optokinetic nystagmus following visual cortical lesions. *Exp. Brain Res.* **88:**594–608.

Fox, P. T., Miezin, F. M., Allman, J. M., Van Essen, D. C., and Raichle, M. E. 1987. Retinotopic organization of human visual cortex mapped with positron-emission tomography. *J. Neurosci.* **7:**913–922.

Freeman, W. J., and Baird, B. 1987. Relation of olfactory EEG to behavior: Spatial analysis. *Behav. Neurosci.* **101:**393–408.

Guillery, R. W., Okoro, A. N., and Witkop, C. J., Jr. 1975. Abnormal visual pathways in the brain of a human albino. *Brain Res.* **96:**373–377.

Guimaraes, A. R., Melcher, J. R., Talavage, T. M., Baker, J. R., Ledden, P., Rosen, B. R., Kiang, N. Y., Fullerton, B. C., and Weisskoff, R. M. 1998. Imaging subcortical auditory activity in humans. *Hum. Brain Mapping* **6:**33–41.

Harris, L. R., Blakemore, C., and Donaghy, M. 1980. Integration of visual and auditory space in the mammalian superior colliculus. *Nature* **288:**56–59.

Hedera, P., Lai, S., Haacke, E. M., Lerner, A. J., Hopkins, A. L., Lewin, J. S., and Friedland, R. P. 1994. Abnormal connectivity of the visual pathways in human albinos demonstrated by susceptibility-sensitized MRI. *Neurology* **44:**1921–1926. [See comments]

Henschen, S. E. 1893. On the visual path and centre. *Brain* **16:**170–180.

Holmes, G. 1918. Disturbances of visual by cerebral lesions. *Br. J. Ophthalmol.* **2:**353–384.

Holmes, G. 1931. A contribution to the cortical representation of vision. *Brain* **54:**470–479.

Holmes, G. 1945. The organization of the visual cortex in man. *Proc. R. Soc. London* **132:**348–361.

Hubel, D., and Wiesel, T. 1962. Receptive fields, binocular interaction and functional architecture of the cat's visual cortex. *J. Physiol.* **160:**106–154.

Hughes, H. C., and Sprague, J. M. 1986. Cortical mechanisms for local and global analysis of visual space in the cat. *Exp. Brain Res.* **61:**332–354.

James, A. C., Mark, R. F., and Sheng, X. M. 1993. Geometry of the projection of the visual field onto the superior colliculus of the wallaby (*Macropus eugenii*). II. Stability of the projection after prolonged rearing with rotational squint. *J. Comp. Neurol.* **330:**315–323.

Knudsen, E. I. 1985. Experience alters the spatial tuning of auditory units in the optic tectum during a sensitive period in the barn owl. *J. Neurosci.* **5:**3094–3109.

Knudsen, E. I., and Brainard, M. S. 1991. Visual instruction of the neural map of auditory space in the developing optic tectum. *Science* **253:**85–87.

Lane, R. H., Allman, J. M., Kaas, J. H., and Miezin, F. M. 1973. The visuotopic organization of the superior colliculus of the owl monkey (*Aotus trivirgatus*) and the bush baby (*Galago senegalensis*). *Brain Res.* **60:**335–349.

Lee, C., Rohrer, W. H., and Sparks, D. L. 1988. Population coding of saccadic eye movements by neurons in the superior colliculus. *Nature* **332:**357–360.

Livingstone, M. S., and Hubel, D. H. 1987. Connections between layer 4B of area 17 and the thick cytochrome oxidase stripes of area 18 in the squirrel monkey. *J. Neurosci.* **7:**3371–3377.

Marotte, L. R. 1990. Development of retinotopy in projections from the eye to the dorsal lateral geniculate nucleus and superior colliculus of the wallaby (*Macropus eugenii*). *J. Comp. Neurol.* **293:**524–539.

Massone, L. L. 1994. A neural-network system for control of eye movements: Basic mechanisms. *Biol. Cybern.* **71:**293–305.

Maunsell, J. H. 1995. The brain's visual world: Representation of visual targets in cerebral cortex. *Science* **270:**764–769.

Mays, L. E., and Sparks, D. L. 1980. Dissociation of visual and saccade-related responses in superior colliculus neurons. *J. Neurophysiol.* **43:**207–232.

Merzenich, M. M., Kaas, J. H., Wall, J., Nelson, R. J., Sur, M., and Felleman, D. 1983. Topographic reorganization of somatosensory cortical areas 3b and 1 in adult monkeys following restricted deafferentation. *Neuroscience* **8:**33–55.

Moschovakis, A. K. 1996. The superior colliculus and eye movement control. *Curr. Opin. Neurobiol.* **6:**811–816.

Pascual-Leone, A., Grafman, J., and Hallett, M. 1994a. Modulation of cortical motor output maps during development of implicit and explicit knowledge. *Science* **263:**1287–1289.

Pascual-Leone, A., Valls, S. J., Wassermann, E. M., and Hallett, M. 1994b. Responses to rapid-rate transcranial magnetic stimulation of the human motor cortex. *Brain,* 847–858.

Pinganaud, G., Pairault, C., and Clairambault, P. 1983. [Retinotopic projections of the trout (*Salmo gairdneri*)]. *J. Hirnforsch.* **24:**15–22.

Poncelet, B. P., Wedeen, V. J., Weisskoff, R. M., and Cohen, M. S. 1992. Brain parenchyma motion: Measurement with cine echoplanar MR imaging. *Radiology* **185:**645–651. [See comments]

Quevedo, C., Hoffmann, K. P., Husemann, R., and Distler, C. 1996. Overrepresentation of the central visual field in the superior colliculus of the pigmented and albino ferret. *Vis. Neurosci.* **13:**627–638.

Reese, T., Davis, T., and Weisskoff, R. 1995. Automated shimming at 1.5 T using echo-planar image frequency maps. *J. Magn. Reson. Imaging* **5:**739–745.

Savoy, R., O'Craven, K., Weisskoff, R., Davis, T., Baker, J., Rosen, B. (1994). Exploring the temporal boundaries of fMRI: measuring responses to very brief visual stimuli. In: Society for Neuroscience 24th Annual Meeting, p. 514–518. Miami Beach.

Sereno, M. I., Dale, A. M., Reppas, J. B., Kwong, K. K., Belliveau, J. W., Brady, T. J., Rosen, B. R., and Tootell, R. B. 1995. Borders of multiple visual areas in humans revealed by functional magnetic resonance imaging. *Science* **268:**889–893. [See comments]

Sereno, M. I., McDonald, C. T., and Allman, J. M. 1994. Analysis of retinotopic maps in extrastriate cortex. *Cereb. Cortex* **4:**601–620.

Somogyvari, Z., Andai, A., Szekely, G., and Erdi, P. 1998. On the role of self-excitation in the development of topographic order in the visual system of the frog. *Biosystems* **48:**215–222.

Sparks, D. L. 1988. Neural cartography: Sensory and motor maps in the superior colliculus. *Brain Behav. Evol.* **31:**49–56.

Sparks, D. L., and Jay, M. F. 1986. The functional organization of the primate superior colliculus: A motor perspective. *Prog. Brain Res.* **64:**235–241.

Sparks, D. L., Lee, C., and Rohrer, W. H. 1990. Population coding of the direction, amplitude, and velocity of saccadic eye movements by neurons in the superior colliculus. *Cold Spring Harbor Symp. Quant. Biol.* **55:**805–811.

Sparks, D. L., and Mays, L. E. 1980. Movement fields of saccade-related burst neurons in the monkey superior colliculus. *Brain Res.* **190:**39–50.

Sparks, D. L., and Mays, L. E. 1983. Spatial localization of saccade targets. I. Compensation for stimulation-induced perturbations in eye position. *J. Neurophysiol.* **49:**45–63.

Sprague, J. M., Berlucchi, G., and Di Berardino, A. 1970. The superior colliculus and pretectum in visually guided behavior and visual discrimination in the cat. *Brain Behav. Evol.* **3:**285–294.

Suga, N., and O'Neill, W. E. 1979. Neural axis representing target range in the auditory cortex of the mustache bat. *Science* **206:**351–353.

Trowe, T., Klostermann, S., Baier, H., Granato, M., Crawford, A. D., Grunewald, B., Hoffmann, H., Karlstrom, R. O., Meyer, S. U., Muller, B., Richter, S., Nusslein-Volhard, C., and Bonhoeffer, F. 1996. Mutations disrupting the ordering and topographic mapping of axons in the retinotectal projection of the zebrafish, *Danio rerio. Development* **123:**439–450.

Van Essen, D. C., Felleman, D. J., DeYoe, E. A., Olavarria, J., and Knierim, J. 1990. Modular and hierarchical organization of extrastriate visual cortex in the macaque monkey. *Cold Spring Harbor Symp. Quant. Biol.* **55:**679–696.